Broadband transmission losses and time dispersion maps from time-domain numerical simulations in ocean acoustics

Alexis Bottero, Paul Cristini, Dimitri Komatitsch, Quentin Brissaud

Broadband transmission losses and time dispersion maps from full-wave time-domain numerical simulations in ocean acoustics

Alexis Bottero,[1, a)] Paul Cristini,[1] Dimitri Komatitsch,[1] and Quentin Brissaud[2]

[1)] *Aix Marseille Univ., CNRS, Centrale Marseille, LMA, Marseille, France.*

[2)] *Division of Geological and Planetary Sciences, Mail Code 252-21, California Institute of Technology, Pasadena, CA 91125, USA.*

bottero@lma.cnrs-mrs.fr

(Dated: 16 May 2018)

Abstract: In this letter, we present a procedure for the calculation of transmission loss maps from time-domain full-wave numerical simulations that can be generalized to arbitrary time sequences and to elastic media. It provides an insight into the understanding of how energy spreads into a complex configuration. In addition, we propose to generate time dispersion maps that give complementary information on how the energy is distributed over time. These maps are generated at a negligible additional numerical cost. To illustrate the kind of results that can be obtained with this procedure, we consider the classical two-dimensional upslope wedge with a fluid bottom and compare our results with those previously obtained based on a parabolic equation. Then, for the same configuration, we present maps for an elastic bottom and for non-monochromatic signals.

[a)] Author to whom correspondence should be addressed.

1. Introduction

In underwater acoustics, several numerical methods are available in the literature for the solution of acoustic wave propagation problems in complex marine environments. Most of them solve the Helmholtz equation, thus providing a frequency-domain solution. This is the traditional way that wave propagation problems in the ocean are handled, and results from these simulations are presented as transmission loss (TL) curves or transmission loss maps. The reason for this choice is the high variability of the ocean, which generates strong signal fluctuations and makes the analysis of time signals difficult. When time-domain solutions are sought, they are often obtained after Fourier transform of the results of several frequency-domain simulations but, in some situations, it may be more convenient to generate the results directly in the time domain. Recently, a time-domain spectral-element method (Komatitsch and Tromp, 1999) has been shown to efficiently solve full-wave propagation problems in ocean acoustics (Bottero *et al.*, 2016; Cristini and Komatitsch, 2012). Beyond its capability of handling complex geometries and rheologies accurately, as any finite-element technique, the time-domain spectral-element method runs efficiently on very large computers, thus providing a drastic reduction of the duration of numerical simulations, which is one of its attractive properties. Nevertheless, this property is partly lost if, instead of the time-domain wave equation, it is the Helmholtz equation that is solved in the framework of a spectral-element method. Consequently, the choice of solving the time-domain wave equation is mandatory to take advantage of the possibility of running such numerical simulations on large supercomputers. The reason for this situation is the behavior of linear system solvers used

for the inversion of the mass matrix when solving in the frequency domain. They typically exhibit decreasing performance when increasing the number of cores and have difficulties scaling when more than a thousand processor cores or so are used. This is a significant limitation because such a number of cores is not that high in terms of current standards, and even less so in the future. Consequently, when solving wave propagation problems requiring a high number of processor cores, the question of the generation of frequency-domain results from time-domain numerical simulations arises, since the underwater acoustics community is used to analyzing results in the frequency domain. A simple way of addressing this question consists in storing all time signals for all receiver positions and then performing a Fourier transform to convert them to the frequency domain. However, this solution is realistic from a technical point of view only if the number of receivers is small to moderate because of the amount of storage (in memory or to disk) that this operation requires when the number of recording points and/or the number of time steps computed are large to very large. In practice, this limits the generation of frequency-domain results from time-domain simulations to the creation of a small number of transmission loss curves, which implies that producing 2D transmission loss maps will require an amount of storage too large to be handled. The objective of this letter is thus to present an efficient way of creating transmission loss maps from time-domain full-wave numerical simulations that avoids the storage of individual time signals. Since the source time signal can be arbitrary chosen, the transmission loss maps can be evaluated for quasi-monochromatic signals as well as for signals with a wider bandwidth, leading to the possibility of analyzing the influence of bandwidth on the distribution of

acoustic energy inside the domain. In addition, time dispersion maps can also be calculated on the fly during the simulation, providing an insight into the structure of the received time signals. All these quantities are obtained at a negligible additional numerical cost.

The letter is organized as follows: Sec. 2 is devoted to the definition of the different physical quantities that we want to study, and to how one can compute them efficiently in a time-domain numerical simulation. Then, in Sec.3, we provide and discuss some examples of the evaluation of these quantities within the framework of a time-domain spectral-element method. Wave propagation over a fluid and then over an elastic upslope wedge is considered for several source bandwidths. We finally draw some conclusions in Sec.4.

2. Generalization of the calculation of transmission losses and evaluation of signal time spreading

In this section, we define the different physical quantities that we want to study and show how they can be calculated on-the-fly in a time-domain full-wave numerical simulation. These quantities will allow for the evaluation of the transmission losses and of the time structure of signals at all the discrete points of the spatial domain under study. Let us note $u_x(\boldsymbol{x},t)$ and $u_z(\boldsymbol{x},t)$ the horizontal and vertical displacement field, respectively, and $P(\boldsymbol{x},t)$ the pressure field at time t and position $\boldsymbol{x}=(x,z)$. $\dot{u}(\boldsymbol{x},t)=\sqrt{\dot{u}_x(\boldsymbol{x},t)^2+\dot{u}_z(\boldsymbol{x},t)^2}$ is the norm of the particle velocity field. The instantaneous energy per unit volume field in the fluid is given by ((Jensen *et al.*, 2011) pp.11-12):

$$\mathcal{E}(\boldsymbol{x},t)=\frac{1}{2}\rho\dot{u}^2(\boldsymbol{x},t)+\frac{1}{2}\frac{P^2(\boldsymbol{x},t)}{\rho(\boldsymbol{x})c^2(\boldsymbol{x})}, \tag{1}$$

where $\rho = 1000$ kg.m^{-3} is the density of water and $c(\boldsymbol{x})$ is the distribution of sound velocity. Likewise, in a linear isotropic solid medium the instantaneous energy field reads (Achenbach, 1973):

$$\mathcal{E}(\boldsymbol{x},t) = \frac{1}{2}\rho(\boldsymbol{x})\dot{u}^2(\boldsymbol{x},t) + \frac{1}{2}\sum_{i,j}\epsilon_{ij}(\boldsymbol{x},t)\sigma_{ij}(\boldsymbol{x},t). \tag{2}$$

where $\epsilon(\boldsymbol{x},t)$ and $\sigma(\boldsymbol{x},t)$ are the second-order strain and stress tensor fields, respectively. Let T_f refer to the duration that is considered, then the integrated energy field reads:

$$E(\boldsymbol{x}) = \int_0^{T_f} \mathcal{E}(\boldsymbol{x},t)\ \mathrm{d}t. \tag{3}$$

This physical parameter represents the amount of energy received at a given position inside the model at time T_f. It is similar to the radiated seismic energy introduced by (Boatwright and Choy, 1986) and evaluated from body waves measurements, or to the T-Phase Energy Flux (TPEF) proposed by (Okal, 2003) to characterize the energy generated by an earthquake source in the form of a T-wave. Then, knowing the energy E_0 of the emitting source, it is possible to evaluate the transmission losses for time T_f as:

$$TL(\boldsymbol{x}) = -10\log\frac{E(\boldsymbol{x})}{E_0} \tag{4}$$

Energy is determined by an integral in time, but with the value that we get we have no knowledge on how this energy is distributed within the time interval that we are considering. For a given energy value, time spreading can be very different depending on the propagation path followed by the signal. It is therefore very useful to get such a piece of information. In

91 order to calculate it, we first define the maximum energy field by:

$$M(\boldsymbol{x}) = \max_{t<T_f} \mathcal{E}(\boldsymbol{x}, t). \tag{5}$$

92 This field gives the maximum of the instantaneous energy for each point and provides a way
93 of defining an "effective" time dispersion for a signal as:

$$\mathcal{T}(\boldsymbol{x}) = 2\frac{E(\boldsymbol{x})}{M(\boldsymbol{x})}. \tag{6}$$

94 This quantity is homogeneous to a duration. It represents the duration of the triangle-shaped
95 signal that has the same energy and maximum amplitude as those that we have calculated. It
96 is therefore a measure of the time spreading of the signal. Time-domain full-wave numerical
97 simulations provide access to these physical parameters at each time step δt and thus allow
98 for the computation of transmission losses and time dispersion maps on-the-fly during the
99 run at a negligible additional computational cost. In practice, at iteration $i+1$ and position
100 $\boldsymbol{x}$, one can evaluate:

$$E_{i+1}(\boldsymbol{x}) = E_i(\boldsymbol{x}) + \mathcal{E}(\boldsymbol{x}, t_{i+1})\delta t \tag{7}$$

101

$$M_{i+1}(\boldsymbol{x}) = \max\left[M_i(\boldsymbol{x}), \mathcal{E}(\boldsymbol{x}, t_{i+1})\right] \tag{8}$$

102

$$\mathcal{T}_{i+1}(\boldsymbol{x}) = 2\frac{E_{i+1}(\boldsymbol{x})}{M_{i+1}(\boldsymbol{x})} \tag{9}$$

103 Time domain full-wave numerical methods can thus also provide an at-a-glance view of how
104 the acoustic energy emitted by a source is distributed inside a complex heterogeneous model.

In the following sections, we will show examples of the maps that can be obtained based on the calculation of these physical quantities.

3. Application to wave propagation in a 2D upslope wedge

In order to validate our approach and to present new results, we choose to investigate the classical two-dimensional (2D) wedge benchmark problem, whose characteristics can be found in Section 6.9.2 of (Jensen *et al.*, 2011). This configuration illustrates several wave propagation phenomena such as mode conversion and mode cutoff due to a varying water column depth. In the context of an attenuating fluid bottom, transmission loss maps for a monochromatic source have already been published and can thus be used for comparison. In addition, with our approach, the transmission loss concept can be extended to broadband source signals and to elastic media. This is an interesting feature that enables us to determine the energy spreading in the whole computational domain. As a consequence these new maps may help to understand the physical mechanisms that lead to the distribution of acoustic energy inside a given configuration. For the sake of illustration, let us first generate a transmission loss map from a full-wave time-domain numerical simulation for exactly the same configuration as in (Jensen *et al.*, 2011). These previous results were obtained with a split-step implementation of the Thomson-Chapman parabolic equation using a Greene wide-angle source to initialize the solution. It is worth noting that the results that will be generated using our approach will be obtained based on a time-domain full-wave numerical simulation that makes no approximation. As a consequence, comparing our results with those obtained with a parabolic equation will also lead to a comparison of the two numerical methods. Then, in

a second step, we will consider the influence of the bandwidth of the emitted signal for both a fluid and an elastic bottom. For this purpose, we define a source time function signal by:

$$s(t) = \begin{cases} \frac{A}{2}\left(1 - \cos\left(\Delta\pi t\right)\sin\left(2\pi f_0 t\right)\right) & \text{if } 0 < t < \frac{2}{\Delta} \\ 0 & \text{else} \end{cases} \tag{10}$$

where A is the maximum amplitude of the source, f_0 is the dominant frequency of the source signal, and Δ is its bandwidth. This type of time sequence will allow us to control the bandwidth of the emitted signal by changing the value of parameter Δ. Quasi-monochromatic signals that will provide results close to frequency-domain calculations as well as narrowband or broadband signals can be generated. We will thus be able to study the influence of the bandwidth on the spreading of acoustic energy inside the computational domain. In addition to a fluid viscoacoustic bottom, we will also consider a solid viscoelastic bottom by adding a shear velocity of $c_s = 600$ m.s^{-1} and a shear attenuation coefficient $\alpha_S = 0.5$ dB.λ_S^{-1} to the sediment characteristics. In the spectral-element method, viscoacoustic or viscoelastic effects are represented based upon three generalized Zener standard linear solids placed in parallel, with different relaxation times for each, to mimic a constant Q quality factor over the frequency band under study in the simulation (Komatitsch and Tromp, 1999). In order to avoid spurious reflections from the sides of the computational domain, for all configurations the domain is extended up to a range of 20 km and down to a depth of 1 km and equipped with perfectly matched absorbing layers (PMLs, (Xie *et al.*, 2016)).

The first results are shown in Fig. 1, which provides the comparison between a monochromatic TL map (Fig. 1(a)) taken from (Jensen *et al.*, 2011) and a quasi-

monochromatic TL map (Fig. 1(b)) generated from a time-domain full-wave numerical simulation.

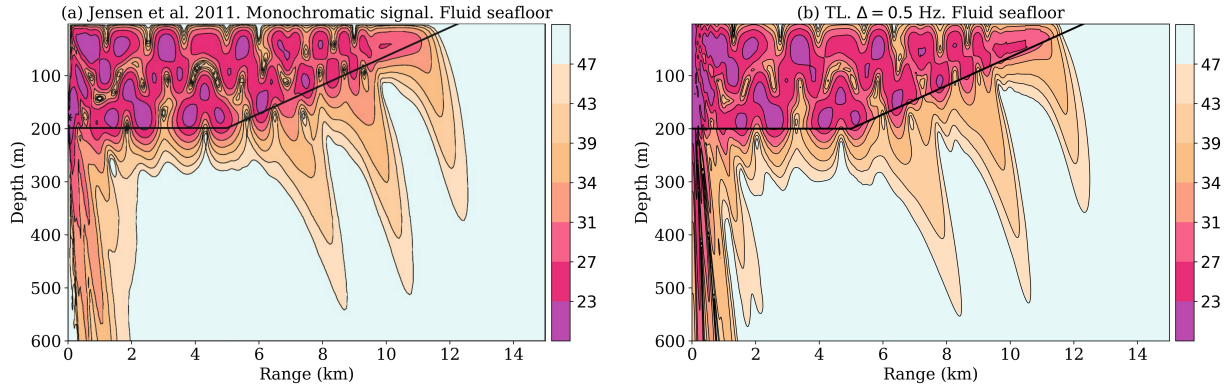

(a) (b)

Fig. 1. (Color online) (a) Original TL map, in dB, from reference (Jensen *et al.*, 2011) page 514. (b) TL map from a full-wave simulation using an quasi-monochromatic source ($f_0 = 25$ Hz, $\Delta = 0.5$ Hz). Figure (a) is reproduced (slightly modified) from Figure 6.11 of (Jensen *et al.*, 2011) with permission from publisher Springer. The black line indicates the seabed interface.

The quasi-monochromatic signal was generated using a bandwidth $\Delta = 0.5$ Hz. We performed several simulations with signals having smaller bandwidth but did not notice any changes in the TL map. We thus consider this value of the bandwidth as a good approximation of a monochromatic signal for this configuration. Note that this is a fluid only configuration. The two TL maps are very similar. Mode cutoff of the three modes, which exist in the flat part of the model, are recovered almost identically in both cases. The main differences are observed for short ranges. This is not surprising since the parabolic equation, which is used to generate the results of Fig 1(a), has angular limitations. Moreover,

a source with a limited aperture was used, contrary to our simulation, which implements a point source. Therefore the discrepancies between the two TL maps are attributed to the known inaccuracy of PE codes for steep angles. Nevertheless, interference structures in the water column are very close, except at the end of the wedge where again the grazing angles are steepened because of the varying depth and thus cannot be handled correctly through numerical modeling based on the parabolic equation. This comparison may be seen as a first answer to the question raised by the author of (Buckingham, 1992) on the accuracy of TL maps obtained using the parabolic equation for an upslope fluid wedge. Based on the results that we obtain, it can be considered that the accuracy is very good.

Since our numerical method works in the time domain, we can also consider signals with different bandwidths in order to evaluate how this parameter may influence the spreading of energy inside the computational domain. Figure 2 (b) represents the TL map for a signal with a bandwidth $\Delta = 8.0$ Hz.

A smoothing of the interference structure is observed in the water column mainly from the beginning of the wedge to its end. The reason for this situation lies in the fact that for each frequency there is a different modal structure, with different grazing angles and therefore different cutoff depths varying continuously with frequency. This smoothing is also observed in the sediment. The complex structure that was observed below the source also disappears.

Adding a shear velocity to the sea floor leads to a very different structure of the leaking of acoustic energy in the bottom (Figure 2 (c)). The leaking of energy associated to

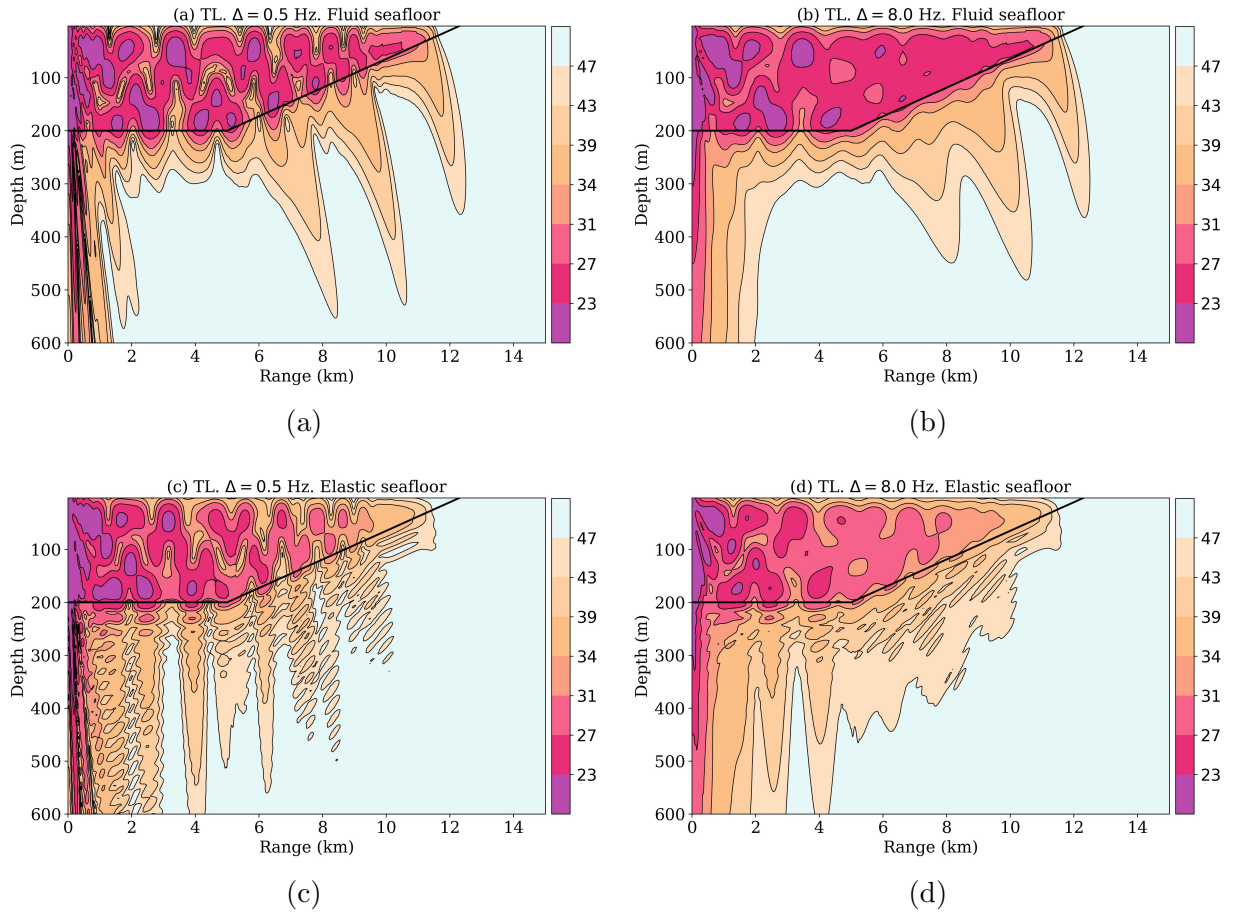

Fig. 2. (Color online) Effect of source bandwidth and bottom elasticity on transmission losses for an upslope wedge. (a) TL map, in dB, for a fluid bottom using a quasi-monochromatic source ($f_0 = 25$ Hz, $\Delta = 0.5$ Hz). (b) TL map, in dB, for a fluid bottom using a broadband source ($f_0 = 25$ Hz, $\Delta = 8.0$ Hz). (c) TL map, in dB, for an elastic bottom using a quasi-monochromatic source ($f_0 = 25$ Hz, $\Delta = 0.5$ Hz). (d) TL map, in dB, for an elastic bottom using a broadband source ($f_0 = 25$ Hz, $\Delta = 8.0$ Hz).

the presence of shear waves is strong and dominant. The associated narrow beams are almost vertical because of the low velocity of shear waves in this configuration. Below the sloping interface, it can be seen that the beams exhibit an interference structure due to the leaking, in this case, of both the shear waves and the propagating modes. This structure is also seen

in the near field but, in this case, it is generated by the leaking of evanescent modes. Similar results were presented in (Abawi and Porter, 2007) (top figure of their Figure 1). It can also be noted that the leaking of the first mode is strongly affected by the presence of shear waves, as it does not penetrate deep into the sediment. There is much less energy in the water column at the end of the wedge than in the fluid-only configuration. A large amount of energy is captured by the shear waves of the bottom. The structure of the sound field in the sediment suggests that if another interface is considered, i.e. if we consider an elastic layer over a semi-infinite half-space, the presence of shear waves is critical and may generate complex effects because of the potential interaction between these beams and this interface. As in the pure fluid case, increasing the bandwidth (Figure 2 (d)) leads to a smoothing of the energy levels mainly in the area of the slope.

As mentioned in the previous section, another type of information can be extracted from time-domain simulations. This piece of information is related to the spreading of energy with time at a receiver location. Indeed, for a given energy level, the time structure of the received signal can be very different and provide additional information on the propagation process that led to this received signal. This is particularly useful e.g. for T-waves analysis because the time structure of a received signal is different depending on the source mechanism that led to the generation of this signal. In order to illustrate the kind of information that is provided by this type of map, we performed a full-wave time domain numerical simulation for a fluid bottom and a broadband signal ($f_0 = 25$ Hz, $\Delta = 25.0$ Hz).

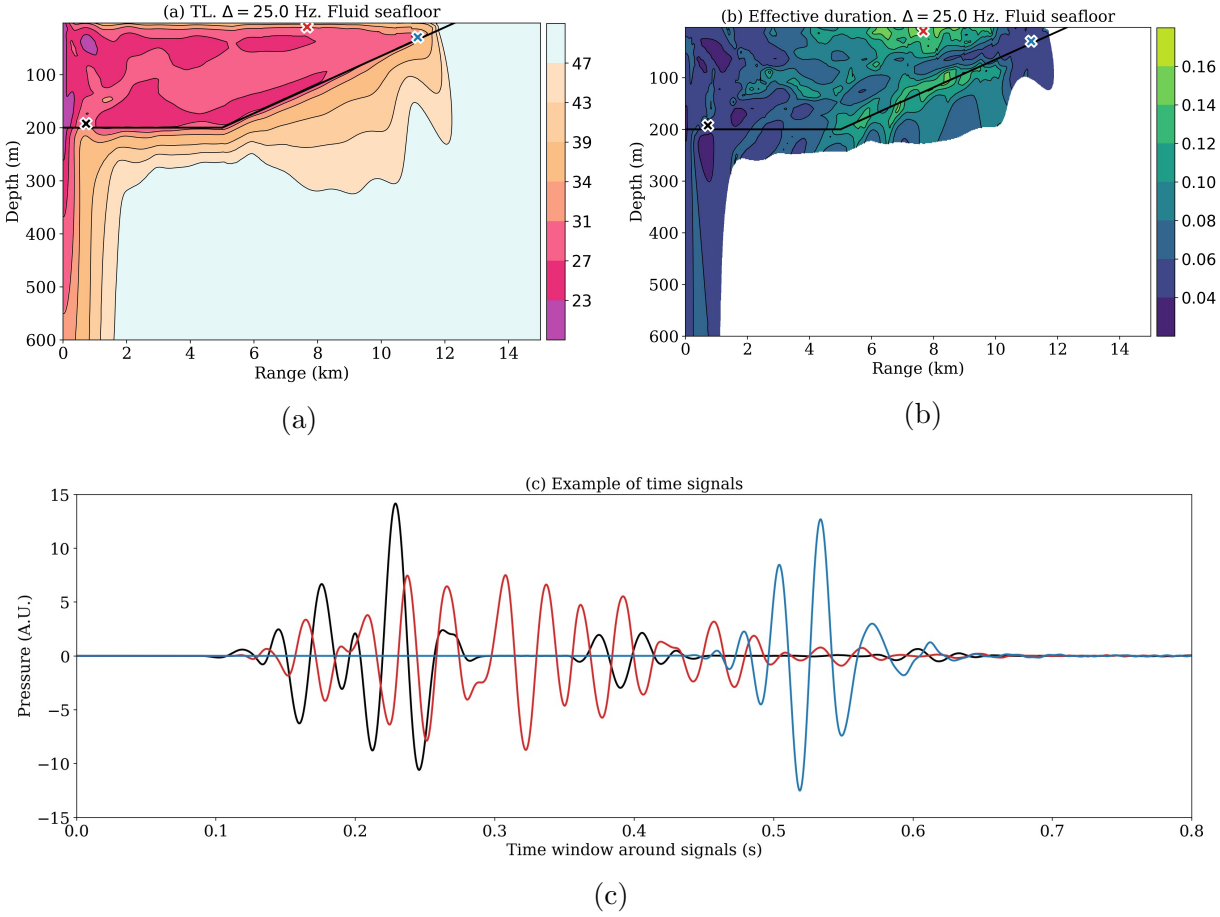

Fig. 3. (Color online) Figure illustrating the use of time dispersion maps. The geometry is the same as in Fig 1. (a) TL map, in dB, using a broadband source (f_0 = 25 Hz, Δ = 25.0 Hz). (b) Associated time dispersion map $\mathcal{T}(\boldsymbol{x})$ (in seconds). This field is shown only for transmission losses that are below 43 dB. (c) Arbitrary time-shifted pressure signals recorded at the positions indicated by the crosses in (a) and (b). The color of each curve corresponds to the color of the respective cross. The wave energy is about the same at the three positions, but the time dispersion is different.

Figure 3 (a) represents the TL map, and Figure 3 (b) represents the time dispersion map for TL values lower than 43 dB only in order to avoid showing very weak signals. Finally, Figure 3 (c) provides time sequences associated to receivers located at the position

of the crosses indicated in Figures 3 (a) and (b). These positions were chosen so that the energy level is similar for all positions. The time sequences are arbitrary shifted for visualization purposes. The time dispersion map exhibits complicated structures reflecting the various time structures that can be generated in this configuration. Signals tend to be more dispersed with range, especially right beneath the sea surface or along the interface with the sea bottom. Nevertheless, at the end of the wedge, at the cutoff depth of mode 1, signals tend to be narrower. This effect is clearly visible in Figure 3 (c).

4. Conclusions

We have presented an efficient procedure to compute transmission losses and time dispersion maps from time-domain full-wave numerical simulations. This procedure allowed us to extend the notion of transmission losses to non-monochromatic signals and to elastic media. Some results using this procedure were obtained for a 2D wedge configuration in ocean acoustics. In the case of a simulation in the frequency domain and for a fluid bottom, these results were compared with results previously obtained using a parabolic equation, showing that both methods give similar results and that the main structures of the sound field are correctly captured by the parabolic equation. Discrepancies between the two approaches were found in regions where the parabolic approximation is known to fail. As a result, our approach can provide reference solutions for more complex configurations because the numerical simulations that are performed are realized without any such approximation and are able to handle complex geometries accurately. In future work we expect to present results

on T-wave propagation or on pile driving, in which this approach may bring new insights into the mechanisms of wave propagation.

Our SPECFEM open source spectral-element software package used in this study is freely available at `geodynamics.org`; it contains all the tools needed to reproduce the simulations presented in this letter.

Acknowledgments

We are grateful to Jean-Pierre Vilotte, Oleg A. Godin and Raphaël F. Garcia for fruitful discussion. The Ph.D. grant of Alexis Bottero was awarded by ENS Cachan, France. This work was granted access to the French HPC resources of TGCC under allocation #gen7165 and of CINES under allocation #A0020407165, both made by GENCI, and of the Aix-Marseille Supercomputing Mesocenter under allocations #b025. We gratefully acknowledge the support of NVIDIA Corporation with the donation of hardware for this research through their Hardware Grant Request program.

References and links

Abawi, A. T., and Porter, M. B. (**2007**). "Propagation in an elastic wedge using the virtual source technique," J. Acoust. Soc. Am. **121**(3), 1374–1382.

Achenbach, J. D. (**1973**). *Wave Propagation in Elastic Solids* (North-Holland, Amsterdam, The Netherlands).

242 Boatwright, J., and Choy, G. L. (**1986**). "Teleseismic estimates of the energy radi-
243 ated by shallow earthquakes," J. Geophys. Res. **91**(B2), 2095–2112, doi: 10.1029/
244 JB091iB02p02095.

245 Bottero, A., Cristini, P., Komatitsch, D., and Asch, M. (**2016**). "An axisymmetric time-
246 domain spectral-element method for full-wave simulations: Application to ocean acoustics,"
247 J. Acoust. Soc. Am. **140**(5), 3520–3530, doi: 10.1121/1.4965964.

248 Buckingham, M. J. (**1992**). *Ocean-acoustic propagation models* (EUR-OP).

249 Cristini, P., and Komatitsch, D. (**2012**). "Some illustrative examples of the use of a spectral-
250 element method in ocean acoustics," J. Acoust. Soc. Am. **131**(3), EL229–EL235, doi:
251 10.1121/1.3682459.

252 Jensen, F. B., Kuperman, W. A., Porter, M., and Schmidt, H. (**2011**). *Computational Ocean*
253 *Acoustics*, 2nd ed. (Springer-Verlag, Berlin, Germany), 794 pages.

254 Komatitsch, D., and Tromp, J. (**1999**). "Introduction to the spectral-element method for 3-D
255 seismic wave propagation," Geophys. J. Int. **139**(3), 806–822, doi: 10.1046/j.1365-246x.
256 1999.00967.x.

257 Okal, E. A. (**2003**). "T waves from the 1998 Papua New Guinea earthquake and its after-
258 shocks: Timing the tsunamigenic slump," Pure Appl. Geophys. **160**(10), 1843–1863, doi:
259 10.1007/s00024-003-2409-x.

260 Xie, Z., Matzen, R., Cristini, P., Komatitsch, D., and Martin, R. (**2016**). "A perfectly
261 matched layer for fluid-solid problems: Application to ocean-acoustics simulations with
262 solid ocean bottoms," J. Acoust. Soc. Am. **140**(1), 165–175, doi: 10.1121/1.4954736.